Supporting Information

Batchelor et al. 10.1073/pnas.1013147107

SI Materials and Methods

Rolipram, 1H-[1,2,4]oxadiazolo[4,3-a]quinoxalin-1-one (ODQ), and N^G-nitro-L-arginine were from Tocris Bioscience; 2-(4-carboxyphenyl)-4,4,5,5-tetramethylimidazoline-1-oxyl-3-oxide (CPTIO), 1-hydroxy-2-oxo-3-(*N*-ethyl-2-aminoethyl)-3-ethyl-1-triazene (NOC-12), diethylammonium (Z)-1-(N,N-diethylamino) diazen-1-ium-1,2-diolate and 2-[(3,4-dimethoxyphenyl)methyl]-7-[(1R)-1-hydroxyethyl]-4- phenylbutyl]-5-methyl-imidazo[5,1-f][1,2,4]triazin-4(1H)-one (BAY 60-7550) were from Axxora UK; 8-bromo-cGMP, 3-isobutyl-1-methylxanthine (IBMX), methoxymethyl-IBMX, Texas red (sulforhodamine 101), and superoxide dismutase were from Sigma-Aldrich, fluorescein was from Millipore, and sildenafil was supplied by the Chemistry Department, Wolfson Institute for Biomedical Research. Common laboratory chemicals were from Sigma-Aldrich.

Cells. The HEK 293T cell lines expressing different levels of guanylyl cyclase (GC) and phosphodiesterase (PDE), called $GC_{high}PDE_{HEK}$, $GC_{high}PDE5_{low}$, and $GC_{mid}PDE5_{high}$ were provided by Doris Koesling (Ruhr-Universität Bochum, Bochum, Germany). For the $GC_{low}PDE_{HEK}$ cell line, the coding sequences of the α1 and β1 GC subunits (*Bos taurus*) were separately inserted into the two independent cloning sites of the vector pBUD CE4.1 (Invitrogen), which permits tandem expression of two cDNA inserts. Originally carried out for a different purpose, the β-subunit was fused at its 3′ end to a sequence encoding the 27 terminal amino acids of syntaxin 3A (*Mus musculus*; Genbank D29797) to target it to the plasma membrane (1). The resulting construct was linearized and lipofected into HEK 293T cells using Fugene (Roche Applied Science). Colonies were selected for 14 d with 300 μg/mL zeocin. Sixty surviving clones were expanded, stimulated with diethylammonium (Z)-1-(N,N-diethylamino)diazen-1-ium-1,2-diolate (10 μM for 10 s) in the absence or presence of ODQ (1 μM), and assayed for cGMP (2). In lysates of the selected clone, NO-stimulated GC activity (measured as in ref. 3 in three independent runs) predominated in the membrane fraction (100,000 × *g* pellet) compared with the cytosol fraction (561 ± 24 vs. 75 ± 3 pmol/mg protein per minute) but the EC_{50} values for NO in the two fractions (measured at 300 μM GTP) were very similar to each other (1.73 ± 0.38 nM and 1.48 ± 0.37 nM, respectively) and to the value found under the same conditions for the protein purified from bovine lung (4). Immunocytochemistry using an antibody directed against the β-subunit showed the protein in transfected HEK cells to be expressed preferentially in the plasma membrane. This localization would not affect the results because intracellular mixing will be extremely rapid relative to the response kinetics: With an intracellular diffusion coefficient of 330 $\mu m^2/s$ (5), cGMP would diffuse the 5-μm radius to the center of a HEK 293T cell (6) in 13 ms. Accordingly, the fluorescent responses appeared uniformly cytoplasmic. All HEK 293T cell lines were maintained under standard conditions in a DMEM-based medium containing 5% fetal bovine serum and appropriate selection antibiotics; they were replated before 80% confluence was reached and were passaged <40 times. Cells growing on poly-D-lysine-coated coverslips were infected with an adenoviral vector expressing δ-FlincG (7) at a dilution of 1:30,000 of a stock at 10^9 pfu/mL (determined by agarose plaque assay) and were used 1–3 d later.

Imaging. Individual coverslips were placed in a small (500 μL volume) chamber mounted on an inverted microscope (Zeiss Axiovert 135TV). The chamber was superfused at 1.5 mL/min with warm (37 °C) solution containing (mM): NaCl (136), KCl (2), $MgSO_4$ (1.2), KH_2PO_4 (1.2), $CaCl_2$ (1.5), glucose (5.5), Hepes (10), N^G-nitro-L-arginine (0.03), superoxide dismutase (100 units/mL), CPTIO (0.1), and uric acid (0.3); the pH was adjusted to 7.4 and the osmolality to 285–290 mosmol kg^{-1}. Inclusion of CPTIO and urate allows the generation of clamped NO concentrations on addition of a slow NO releaser (3), in this case, NOC-12 (half-life = 100 min at 37 °C and pH 7.4). Clamped NO concentrations were applied to the cells in two ways. Initially, they were delivered by superfusion. Fluorescein (0.1–1 nM) was delivered in the same way at the end of these experiments to estimate the dead space of the perfusion line (all traces are corrected for this delay) and to quantify the mixing time in the chamber (see Fig. S5). Secondly, for more rapid "puff" applications, a glass pipette was pulled to a point (tip diameter ≈ 5 μm) and clamped NO solution in the pipette (1 nM) was ejected by a pressure pulse (1–5 psi, 0.1–30 s duration), switched with solenoid valves (Picospritzer IID, General Valve Corp.), under the control of an external timer (Master-8, AMPI). Texas red dye (10 μM) was included in the pipette solution to allow the spread of the pipette solution to be imaged and quantified (see Fig. S5). Mixing of the expelled puff with the recipient perfusing solution is assumed to affect the constituents of the pipette solution equally. The bath perfusing solution contained CPTIO at the same concentration as in the expelled solution and mixing would reduce the concentrations of NO and the NO donor by the same amount. NO would then immediately be at a new clamped concentration that is proportional to the degree of dilution (3).

Optics. The wavelengths and intensities of light used to excite the samples were supplied by a combined filter wheel/lamp/variable aperture shutter (Lumen200Pro, Prior Scientific Instruments) which was coupled to the epifluorescence port of the microscope by a liquid light guide. Dual-band imaging of δ-FlincG (excitation at 470/40 nm; peak transmittance/width at half-maximal transmittance) and Texas red (572/35 nm) used a custom-coated beamsplitter and emission filter (Chroma Technology). Images were captured by a camera (Rolera-XR, Q-Imaging) under software control (ImagePro 6.3, MediaCybernetics). The exposure, binning, camera gain, acquisition rate, and light intensity were optimized to achieve a large signal–noise ratio while minimizing bleaching, phototoxicity, and light-induced NO-release (see Fig. S6).

Analysis. Cellular fluorescence was corrected for the background level and displayed as the change in intensity relative to baseline divided by the baseline intensity ($\Delta F/F_0$). Usually several cells were averaged and the results are presented as means ± SEM. During the longer experiments, the fanning out of baselines (apparently randomly) generated increasing errors with time when traces from several cells were averaged. To avoid this distortion, individual traces were usually corrected for drift by subtracting straight lines connecting prestimulation baselines (as illustrated for a single cell in Fig. 1*A*) prior to averaging. This procedure was used for the data shown in Figs. 1, 3, and 5, and Figs. S2*C*, S3*A*, and S4 *A–C* (but not others). Conversion of δ-FlincG fluorescence into cGMP concentrations used the rearranged Hill equation

$$[\text{cGMP}] = EC_{50}\left(\frac{r}{R_{max} - r}\right)^{1/n}, \qquad \textbf{[S1]}$$

where EC_{50} is the cGMP concentration giving half-maximal δ-FlincG fluorescence (0.17 μM; ref. 7), r is the δ-FlincG response, R_{max} the maximum δ-FlincG response, and n is the Hill slope (1.45, from figures 1 and 4 of ref. 7). Modeling of the data was carried out using Mathcad 14 (Parametric Technology Corporation). The GC component was modeled as in Fig. 2*A*. PDE_{HEK} was taken to be a Michaelis–Menten-type enzyme (see *Results*) obeying the following relationship:

$$v_d = \frac{PDE_{max}[cGMP]}{K_p(1 + [I]/K_I) + [cGMP]}, \quad \textbf{[S2]}$$

where v_d = rate of cGMP hydrolysis, PDE_{max} = maximum rate of cGMP hydrolysis, K_p = apparent Michaelis constant, $[I]$ = competitive antagonist concentration, and K_I = competitive antagonist dissociation constant. A range of values of K_p (1–10 μM, with balancing adjustments to PDE_{max}) could adequately describe the observed rates of hydrolysis, the best overall value (describing the data in Figs. 1*B* and 3*A*, and Figs. S3*A* and S4 *A–D*) being about 4 μM, which was the one used in the simulations. The values of PDE_{max} were adjusted to obtain the best fits for each experiment based on the sum of the squares of the errors. The phosphodiesterase (PDE) 5 kinetic parameters (Fig. 2*B* and Table 2) were obtained from four experiments in which a series of four NO puffs was delivered to $GC_{high}PDE5_{low}$ cells, followed by test puffs at various intervals up to 10 min (Fig. 4). The data were sufficiently rich in information that values of all the parameters, together with GC_{max}, PDE_{max}, K_p, and the background rate of cGMP formation (see *Results*), could be computed from each experiment using the Levenberg–Marquardt method (the "Minerr" function in Mathcad), which is based on minimizing the sum of the squares of the errors between theory and experiment. Attempts were made to incorporate a basal PDE5 activity of the cGMP-free species but this activity was found to be negligible (<5% of the maximal activity of the cGMP-bound states), in agreement with findings with rat platelets (8), and so was ignored. Particularly with briefer puffs, the concentration of NO reached inside the cells will be partially limited by diffusion through the unstirred layers inside and surrounding them. Although this factor had a relatively small influence (Fig. 5*B*, *Inset*), a better fit to the data was obtained if it was included. A rate constant for diffusion through the unstirred layers of 49 s^{-1} gave the best overall result; assuming the cells to be spherical with a radius of 5 μm, and intracellular and extracellular NO diffusion coefficients of 848 and 3,300 $\mu m^2/s$, respectively (9), this rate constant corresponds to an extracellular unstirred layer of 13-μm thickness (calculated according to ref. 10), which is reasonable for cultured cells subjected to rapid stirring (11). In addition, in the puff experiments, the concentration of NO receptors in the cells will influence the intracellular NO concentration dynamics and so, for analyzing the data, the receptor concentration was derived by assuming a GC turnover number of 50 s^{-1}, which was based on pure NO-activated GC having a molecular mass of 150 kDa and a maximal activity of 20 $\mu mol \cdot mg^{-1} \cdot min^{-1}$. Multiplying the receptor concentration by the turnover number gives the GC_{max} values incorporated into Table 1. The mean NO receptor concentration in the $GC_{high}PDE5_{low}$ cells subjected to NO puffs came to 0.437± 0.095 μM ($n = 7$). The final values of the PDE5 kinetic parameters (Table 2) were reached in three steps. First, from the response recovery data (e.g., Fig. 4*C*), a tentative value was assigned to k_{-3} based on the mean computer-generated estimates from eight runs covering different recovery times in four separate experiments [$(1.98 \pm 0.16) \times 10^{-3}$ s^{-1}]. After fixing this value, and reanalyzing the data, the parameter with the lowest error was the apparent Michaelis constant (K_p) which was then fixed. The ratio of kp_{-3} to kp_3 then had the lowest error [$(1.60 \pm 0.49) \times 10^{-9}$ M; $n = 13$], allowing a tentative value for kp_3 to be allocated (1.30×10^5 M^{-1} s^{-1}). With these values in hand, the second step was to analyze the averaged four-puff induction phases of each experiment, which allowed the parameters kp_{-1}, kp_{-2}, kp_2, and kp_1 to be fixed in that order, based on lowest errors. The only constraint applied was that $kp_2 > kp_{-2}$, to exclude fitting in some runs to a very low efficacy PDE($kp_2/kp_{-2} \approx 0.06$) that would be incompatible with other data. Finally, reanalysis of the recovery experiments produced the final values of kp_3 and kp_{-3} (fixed in that order). The background GC activity (see *Results*), GC_{max}, and PDE_{max} were treated as variables throughout. The mean background GC activity was 6.52 ± 0.82 nM/s ($n = 4$), corresponding to an average NO concentration of 3.26 pM; values for GC_{max} and PDE_{max} in different experiments are given in the figure legends and/or are included in Table 1. To account for the shapes of initial responses in the puff experiments, it was usually necessary to incorporate a finite initial level of pPDE5* (typically 0.1–2% of total), presumably the result of prior exposure to environmental NO or to test NO puffs. Attempts were made to determine if the kinetic parameters (PDE_{max} or K_p) of the two active PDE5 species (tPDE5* and pPDE5* in Fig. 2*B*) might differ. These tests used the averaged four-puff induction phases and were carried out by fixing one parameter and allowing the other to adopt a distinct value for each PDE5 species. The background GC, GC_{max}, and (when searching for distinct K_p values) PDE_{max} values were allowed to vary. With K_p fixed (at the global mean of 0.35 μM; Table 2), the ratio of PDE_{max} values for the two species (pPDE5*/tPDE5*) came to 0.83 ± 0.09 ($n = 4$); with PDE_{max} fixed to be the same for the two species, the corresponding ratio of K_p values was 1.18 ± 0.35 ($n = 4$). Neither ratio is significantly different from unity ($P = 0.14$ and 0.64, respectively) and the mean K_p for both species (0.31 ± 0.05 μM; $n = 8$) was not significantly different ($P = 0.44$) from the global mean (0.35 μM; Table 2). Hence, the two active PDE5 species were allocated the same kinetic parameters. [Note: With the designated parameters, it is implicit in the mechanism that the total available PDE5 activity and the agonist potency of cGMP will both increase on formation of the pPDE5* species, in accordance with observations of the effect of phosphorylation on isolated recombinant bovine PDE5 (12).]

1. Watson RT , Pessin JE (2001) Transmembrane domain length determines intracellular membrane compartment localization of syntaxins 3, 4, and 5. *Am J Physiol Cell Physiol* 281:C215–C223.
2. Gibb BJ, Wykes V, Garthwaite J (2003) Properties of NO-activated guanylyl cyclases expressed in cells. *Br J Pharmacol* 139:1032–1040.
3. Griffiths C, Wykes V, Bellamy TC, Garthwaite J (2003) A new and simple method for delivering clamped nitric oxide concentrations in the physiological range: Application to activation of guanylyl cyclase-coupled nitric oxide receptors. *Mol Pharmacol* 64:1349–1356.
4. Roy B, Halvey EJ, Garthwaite J (2008) An enzyme-linked receptor mechanism for nitric oxide-activated guanylyl cyclase. *J Biol Chem* 283:18841–18851.
5. Huang RC, Gillette R (1991) Kinetic analysis of cAMP-activated Na^+ current in the molluscan neuron. A diffusion-reaction model. *J Gen Physiol* 98:835–848.
6. Thomas P, Smart TG (2005) HEK293 cell line: A vehicle for the expression of recombinant proteins. *J Pharmacol Toxicol Methods* 51:187–200.
7. Nausch LW, Ledoux J, Bonev AD, Nelson MT, Dostmann WR (2008) Differential patterning of cGMP in vascular smooth muscle cells revealed by single GFP-linked biosensors. *Proc Natl Acad Sci USA* 105:365–370.
8. Mo E, Amin H, Bianco IH, Garthwaite J (2004) Kinetics of a cellular nitric oxide/cGMP/phosphodiesterase-5 pathway. *J Biol Chem* 279:26149–26158.
9. Liu X, et al. (2008) Nitric oxide diffusion rate is reduced in the aortic wall. *Biophys J* 94:1880–1889.
10. Hardt SL (1979) Pace of diffusion through membranes. *J Membr Biol* 48:299–323.
11. Spivak CE, Oz M, Beglan CL, Shrager RI (2006) Diffusion delays and unstirred layer effects at monolayer cultures of Chinese hamster ovary cells: Radioligand binding, confocal microscopy, and mathematical simulations. *Cell Biochem Biophys* 45:43–58.
12. Corbin JD, Turko IV, Beasley A, Francis SH (2000) Phosphorylation of phosphodiesterase-5 by cyclic nucleotide-dependent protein kinase alters its catalytic and allosteric cGMP-binding activities. *Eur J Biochem* 267:2760–2767.

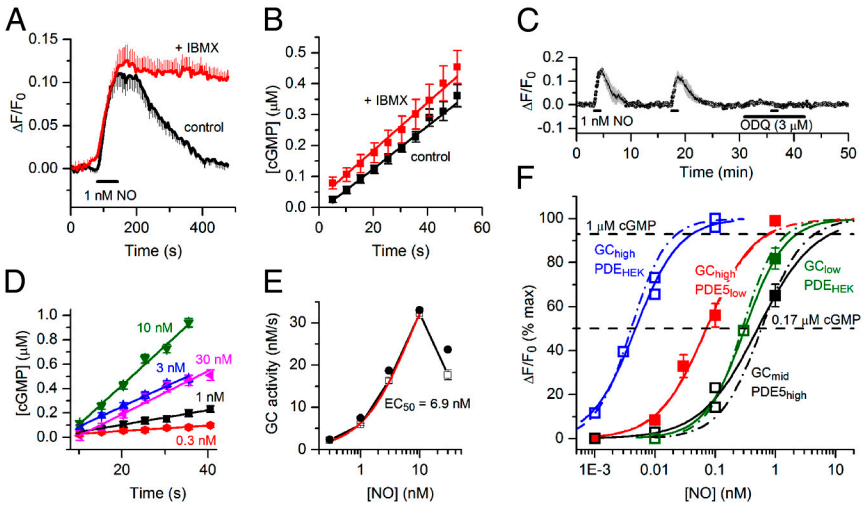

Fig. S1. NO concentration-response relationships in model cells. (*A*) The δ-FlincG response in $GC_{low}PDE_{HEK}$ cells on superfusion of 1 nM NO before (control) and 6.6 min after addition of the nonselective PDE inhibitor IBMX (100 μM; five cells) showing that the rising phases of the responses (recorded 22 min apart) superimpose despite the substantial difference in decay rates. (*B*) The rising phases of δ-FlincG responses to 1 nM NO in four experiments (three to nine cells in each), performed as in *A*, were converted into cGMP concentrations (see *SI Materials and Methods*); the slopes of linear fits (control, 7.75 ± 1.24 nM/s; +IBMX, 8.37 ± 0.67 nM/s) were not significantly different ($P = 0.66$ by paired *t* test), showing that the PDE activity makes a negligible contribution to the upstroke of the response. (*C*) Inhibition of response to 1 nM NO in $GC_{low}PDE_{HEK}$ cells by ODQ (three cells). (*D*) δ-FlincG responses from $GC_{low}PDE_{HEK}$ cells during perfusion of different NO concentrations (data in Fig. 1), after conversion into cGMP concentrations, were fitted to linear functions. The slopes of the lines (with computer-derived errors) are plotted against NO concentration in *E* (open symbols), the red line being a fit of the rising phase to the Hill equation, giving the stated EC_{50} value; filled symbols are from analyzing the model output (with $GC_{max} = 0.235$ μM/s and $PDE_{max} = 0.036$ μM/s; see Fig. 1) in the same way. (*F*) Amplitudes of δ-FlincG responses to different NO concentrations in all four model cells possessing different mixtures of GC and PDE activities, normalized to the maximum amplitude. The amplitudes corresponding to 0.17 μM (the EC_{50}) and 1 μM cGMP, based on the properties of δ-FlincG, are indicated by horizontal broken lines. Open symbols are individual experiments (averaging 13 cells each); filled symbols are means (±SEM where visible) of three to five experiments. Solid lines are Hill fits to the experimental data, dot-dash lines are computed Hill fits to data from the model for NO-activated GC (Fig. 2*A*) together with the appropriate PDE type, using the mean GC_{max} and PDE_{max} values found for the experimental data (Table 1).

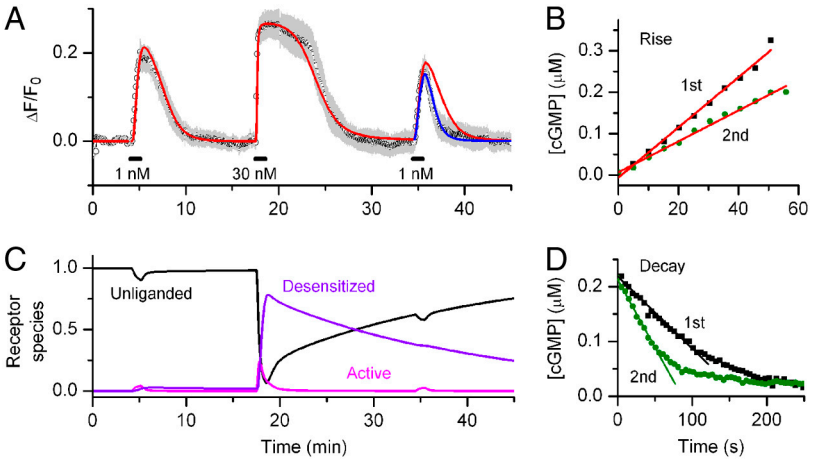

Fig. S2. Plasticity following exposure of $GC_{low}PDE_{HEK}$ cells to a high (30 nM) NO concentration. (*A*) $GC_{low}PDE_{HEK}$ cells ($n = 5$) were superfused twice with 1 nM NO (1 min), with exposure to 30 nM NO (1 min) in between. The red line is a fit to the model with $GC_{max} = 0.25$ μM/s and $PDE_{max} = 0.05$ μM/s; for the blue line, PDE_{max} was raised to 0.09 μM/s from the start of the final response. The underlying alterations in the principal NO receptor species, according to the model, are shown in *C*, where (referring to Fig. 2*A*), Unliganded, GC; Active, NOGC*; and Desensitized, GC*NO. (*B*) Conversion of the rising phases (mean data) of the two responses to 1 nM NO into cGMP concentrations, showing desensitization; the lines are linear fits, from which the amount of desensitization is calculated to be 38%. (*D*) Similar treatment of the falling phases showing speeding of the decay, signifying increased PDE activity (by 90% based on the superimposed linear fits to the initial decays).

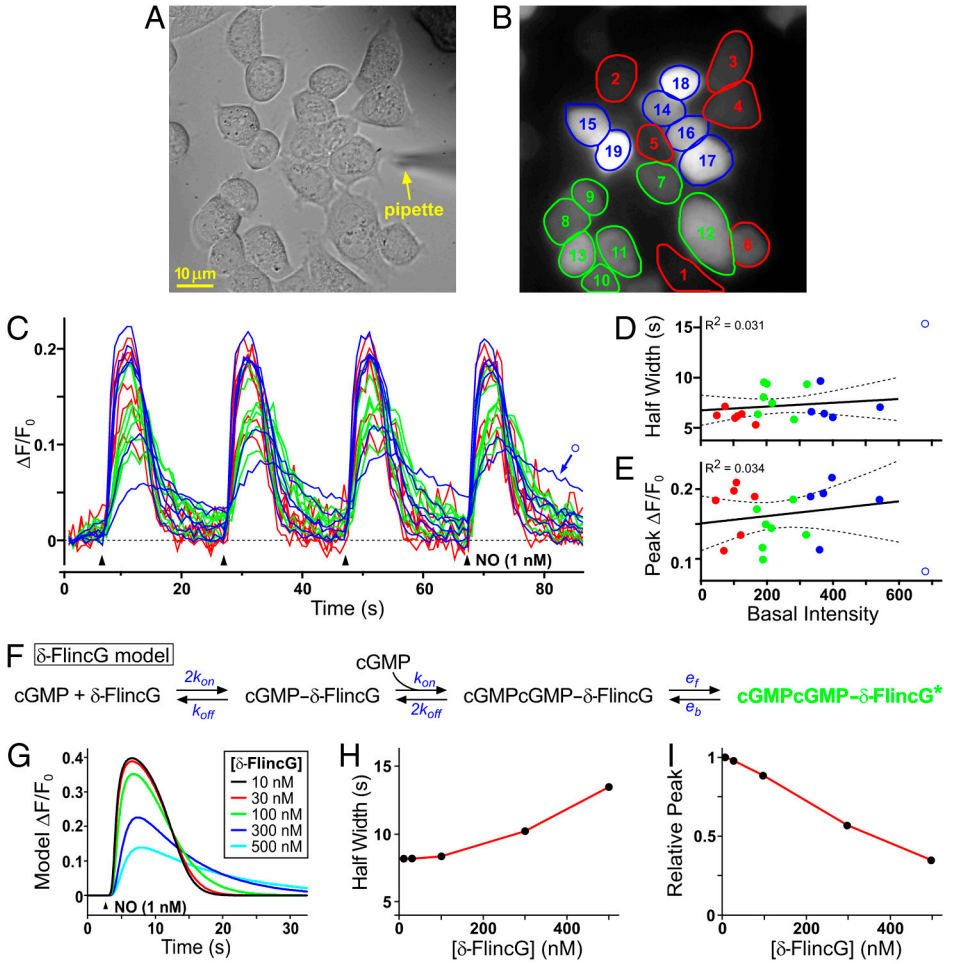

Fig. S3. Evaluation of δ-FlincG for recording cGMP dynamics. (*A*) Brightfield image of $GC_{high}PDE5_{low}$ cells showing position of puffer pipette. (*B*) Range of basal δ-FlincG fluorescence in the field shown in *A*. Numbers refer to fluorescence intensity ranked from low to high and are grouped into low (red outline), medium (green outline), or high (blue outline) intensities. (*C*) Response of the cells to NO (1 nM in pipette, four 1-s puffs at 20-s intervals), color-coded as in *B*. (*D* and *E*) Linear regression analysis of the first response indicates that neither the width at half height (*D*) nor peak amplitude (*E*) of the $\Delta F/F_0$ signal was significantly correlated with the basal δ-FlincG fluorescence, presumed to reflect the amount of δ-FlincG protein ($P = 0.49$ and 0.47, respectively; broken lines are 95% confidence limits). Symbols are color-coded to match *B* and *C*; the open symbol represents the one apparent outlier (identified in the same way in *C*) which was excluded in the regression analyses in *D* and *E*. (*F*) Model of δ-FlincG kinetics. For simplicity, it is assumed that the two cGMP binding sites (7) have the same properties and are independent, and that both sites need to be occupied to generate a change in fluorescence. The steady-state EC_{50} is given by

$$EC_{50} = \frac{K_d[(E+2)^{0.5}+1]}{1+E}, \qquad \text{[S3]}$$

where $K_d = k_{off}/k_{on}$ and $E = e_f/e_b$. Rate constants ($k_{on} = 5 \times 10^7$ M^{-1} s^{-1}, $k_{off} = 6.825$ s^{-1}, $e_f = 22$ s^{-1}, $e_b = 17.6$ s^{-1}) were assigned to give the measured EC_{50} for cGMP (0.17 μM), deactivation rate (half-time = 0.16 s), and association kinetics at different cGMP concentrations (figure 3 of ref. 7). The predicted Hill slope of the steady-state cGMP concentration-δ-FlincG response curve comes to 1.37, which is consistent with the experimental data (the mean value from figures 1 and 4 in ref. 7, ≈1.45). (*G*) Predicted effect of δ-FlincG concentration on the fluorescent signal dynamics, carried out by combining the δ-FlincG model (*F*) with the GC/PDE5 model for these cells (see main text) and simulating the NO puff used in *C*. Marked increases in the response width and reductions in the peak amplitude are predicted at δ-FlincG concentrations of 300 nM or more (plotted in *H* and *I*, respectively). It can be concluded that, with the possible exception of one cell (number 19 in *B*; open symbol in *C*, *D*, and *E*), that the δ-FlincG concentration inside the cells is likely to be 200 nM or less, and that the presence of the biosensor does not measurably distort the cGMP dynamics.

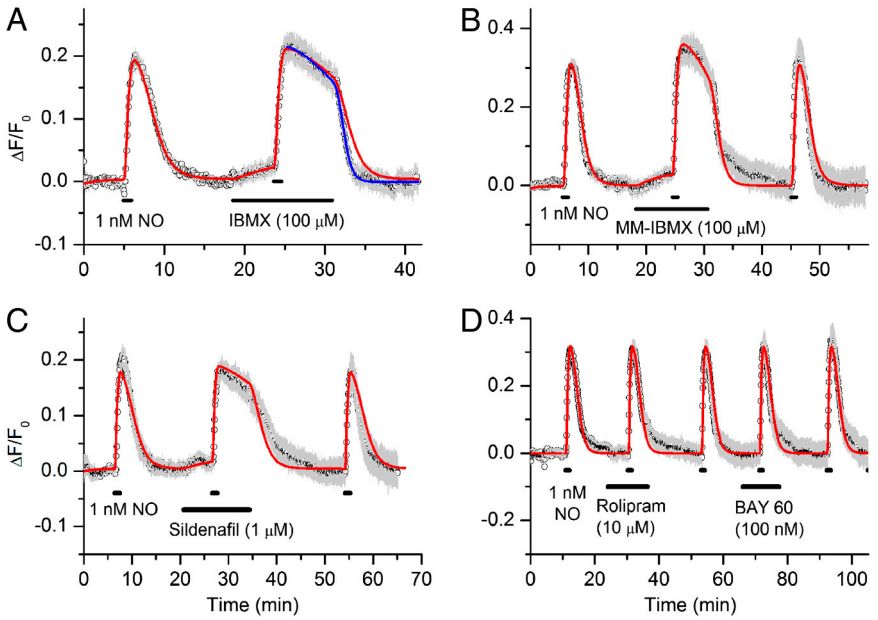

Fig. S4. Pharmacological properties of PDE_{HEK}. $GC_{low}PDE_{HEK}$ cells were superfused with 1 nM NO (1 min) with or without the nonselective PDE inhibitor IBMX (*A*, nine cells; see also Fig. S1), its methoxymethyl derivative [*B*, methoxymethyl (MM)-IBMX, 17 cells] that is partially selective for PDE1, sildenafil (*C*, six cells), which inhibits PDE5 more potently than PDE1 (IC_{50} = 10 nM vs. 0.35 μM; ref. 1), and the PDE4- and PDE2-selective inhibitors rolipram and BAY 60-7550 (BAY 60), respectively (*D*, 15 cells). The red lines are fits to the model, assuming GC_{max} = 0.22–0.35 μM/s and PDE_{max} = 0.035–0.060 μM/s. To account for the small, slow rise in fluorescence on adding the inhibitors in *A*–*C*, a low background rate of cGMP formation averaging 160 ± 36 pM/s (n = 8) was included. Fitting the effects of the inhibitors on the response to 1 nM NO gave K_I values of 30 μM for MM-IBMX (n = 1), 0.3 and 0.4 μM for sildenafil (n = 2), and 23.8 ± 4.3 μM for IBMX (n = 4). In all experiments with IBMX (e.g., *A*), the fluorescence decay was faster after washout of the inhibitor and the responses were better fitted assuming that PDE_{max} increased during the exposure to NO from 0.046 ± 0.004 μM/s to 0.080 ± 0.003 μM/s (n = 4; blue line in *A*). Reanalysis with the increased values of PDE_{max} gave a K_I for IBMX of 11.8 ± 3.2 μM. This pharmacology is most consistent with PDE_{HEK} being a PDE1 isoform (1), although a mixture of PDEs (e.g., PDE1 plus PDE5) could also be operative.

1 Bender AT, Beavo JA (2006) Cyclic nucleotide phosphodiesterases: Molecular regulation to clinical use. *Pharmacol Rev* 58:488–520.

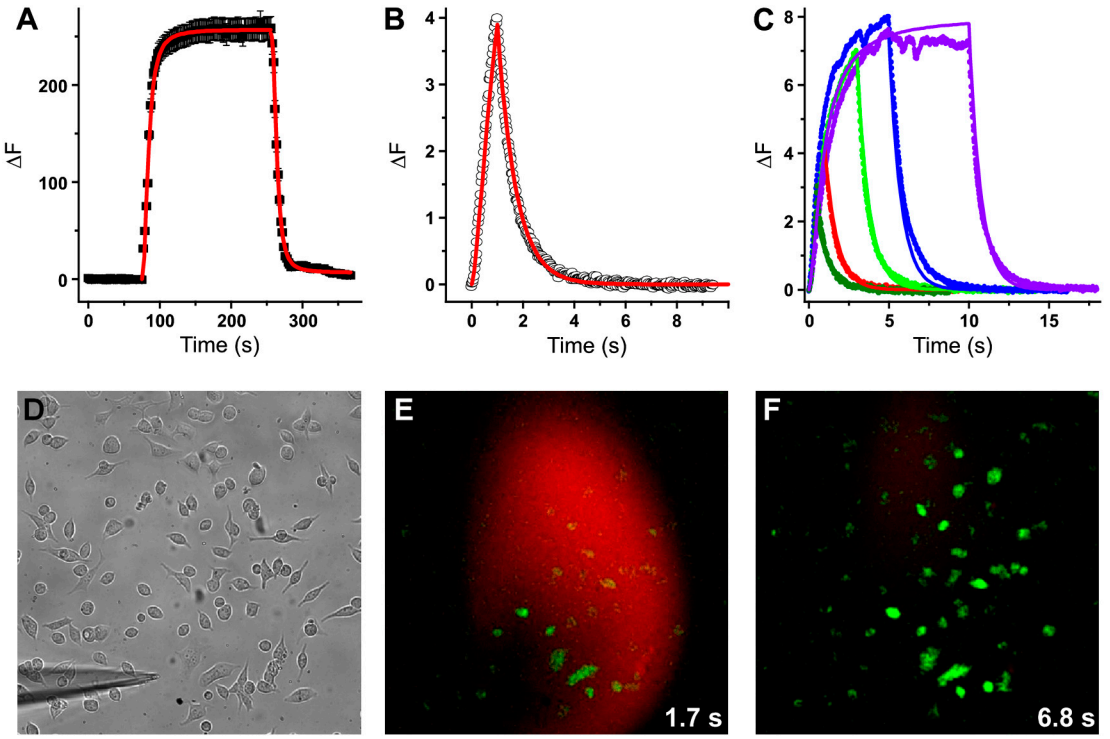

Fig. S5. Quantification of NO exposures. (*A*) Typical change in fluorescence following wash-in and washout of fluorescein by perfusion. The increase and decrease in fluorescence were both fitted (red lines) by a logistic function:

$$y = A2 + \frac{(A1 - A2)}{(1 + \frac{t}{t0})^p}, \quad \textbf{[S4]}$$

where y is the fluorescence amplitude, $A1$ and $A2$ are the initial and final fluorescence amplitudes, respectively, t is the time, $t0$ is the half-time, and p is the slope factor. In this experiment, the points are means of 10 fields; for the rising phase, $t0 = 8.94$ s and $p = 2.19$, and, for the falling phase, $t0 = 8.73$ s and $p = 2.61$. (*B* and *C*) Texas red fluorescence over a cell of interest following application of puffs lasting 1 s (*B*) or 0.5–10 s (*C*). The Texas red was mixed with the clamped NO concentration in the pipette. The rising phases were fitted by a logistic function (red line in *B*, $t0 = 0.945$ s and $p = 1.565$) and the falling phase by a single exponential: $y = A1 \cdot \exp(-k.t)$, where $A1$ is the amplitude and k is the decay constant (1.392 s^{-1} in *B*; red line). In *C*, the kinetics of a range of puff durations was analyzed individually and the mean parameters (maximum amplitude = 8.0, $t0 = 0.947$ s, $p = 1.557$, $k = 1.349$ s^{-1}) give a reasonable fit (lines) to all the traces. Assuming that NO and the dyes spread comparably, the calibrations allow the NO exposures in the two types of experiment to be quantified and simulated for modeling purposes (see *SI Materials and Methods*). (*D–F*) Images from sample experiment with application of an NO puff lasting 3 s. (*D*) Brightfield image showing position of puffer pipette. (*E* and *F*) Texas red (red) and δ-FlincG (green) fluorescence 1.7 s (*E*) and 6.8 s (*F*) after initiating the puff. For the purposes of illustration, a lower than normal magnification (×10 instead of ×40 objective) was used to show the spread of the puff (see Movie S1).

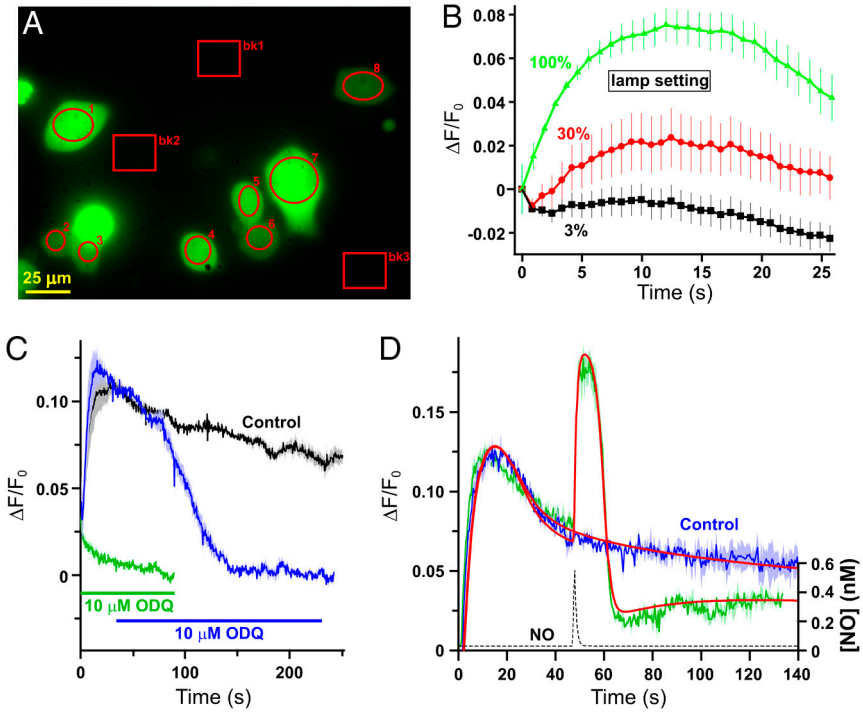

Fig. S6. Light-induced NO-release. The experiments were designed to find the origin of the increase in δ-FlincG fluorescence observed when imaging at higher frame rates without added NO. (*A*) Fluorescent image of δ-FlincG-expressing $GC_{high}PDE5_{low}$ cells indicating analysis regions (numbered ellipses) and areas for background subtraction (bk1–3). (*B*) The mean intensity of the regions is displayed as $\Delta F/F_0$ (±SEM; $n = 8$). The light intensity at the cells was varied by controlling the aperture (nominal percentage settings) which regulates the light entering the liquid light guide. Only the camera gain was altered to keep the intensity within range. The interval between frames was 0.84 s. (*C*) Inhibition of the fluorescence increase taking place during imaging (control, four cells) by previous incubation in ODQ (green line, four cells) or by addition of ODQ near the response peak (blue line, 3 cells), implying that the increased fluorescence is caused by NO-activated GC. (*D*) Long-term suppression of the response (two cells) as a result of giving an NO puff (1-s puff; 1 nM NO in the pipette). The data are modeled (red lines) with $GC_{max} = 42.5$ µM/s and $PDE_{max} = 2.5$ µM/s and, to match the control fluorescence, with a background NO concentration of 30 pM (broken black line). The results in *C* and *D* were acquired at 1 frame every 0.46 s. The findings suggest that the response is the result of light-induced release of NO, a phenomenon that can be traced back more than 40 y (1) and which could be ascribed to photodecomposition of nitrosothiols and/or nitrite (2) and/or nitrate (3). In subsequent experiments, light exposure was adjusted to minimize its contribution.

1 Ehrreich SJ , Furchgott RF (1968) Relaxation of mammalian smooth muscles by visible and ultraviolet radiation. *Nature* 218:682–684.
2 Rodriguez J, Maloney RE, Rassaf T, Bryan NS, Feelisch M (2003) Chemical nature of nitric oxide storage forms in rat vascular tissue. *Proc Natl Acad Sci USA* 100:336–341.
3 Dejam A, et al. (2003) Thiols enhance NO formation from nitrate photolysis. *Free Radical Biol Med* 35:1551–1559.

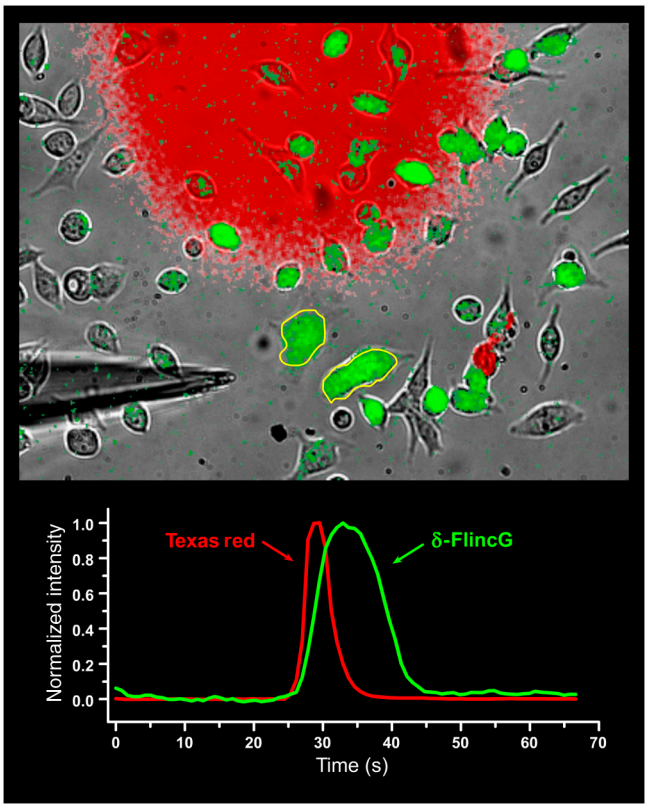

Movie S1. Coimaging of Texas red and δ-FlincG fluorescence in a field of $GC_{high}PDE5_{low}$ cells. A single puff (3-s duration) was delivered from a pipette containing Texas red and 1 nM clamped NO. The traces below are averages from the two cells outlined in yellow.

Movie S1 (MOV)

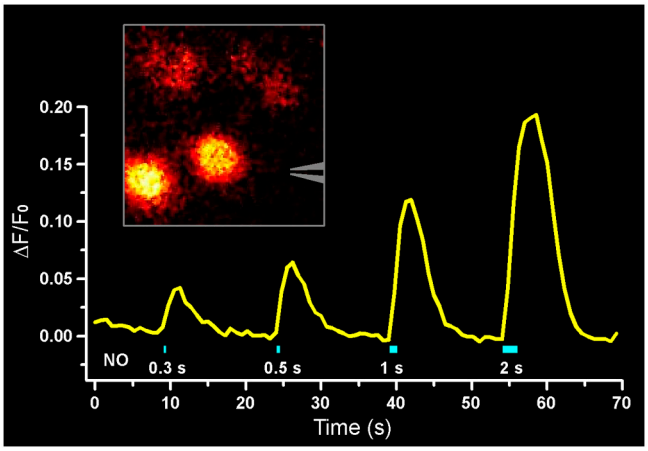

Movie S2. Dynamics of cellular NO detection by $GC_{high}PDE5_{low}$ cells expressing δ-FlincG. The *Inset* shows a group of cells showing transient increases in fluorescence in response to puffs of NO of lengthening duration. The position of the puffer pipette (containing 1 nM clamped NO) is indicated (gray). The main panel charts the average fluorescence (yellow) in two of the cells (the two brightest ones in the *Inset*); the durations of the NO puffs are given underneath the trace.

Movie S2 (MOV)